Helical Motion Analysis of the 2-Degree-of-Freedom Split-Stator Induction Motor

Lujia Xie[1,3], Jikai Si[2], Yihua Hu[1], *senior member, IEEE*, and Haichao Feng[4]

[1] University of Liverpool, Department of Electrical Engineering and Electronics, Liverpool, UK
[2] Zheng Zhou University, College of Electric Engineering, Henan, Zheng Zhou, China
[3] Department of Electrical Engineering, National Tsing Hua University, Hsinchu 30013, Taiwan
[4] Henan Polytechnic University, School of Electrical Engineering and Automation, Jiaozuo, Henan, China

In this paper, the characteristics of the helical motion of the rotatory-linear 2-degree-of-freedom split-stator induction motor (2DoFSSIM) are investigated, which cannot be regarded as the simple superimposition of the 1DoF rotary and linear motions. A set of torque and force equations of helical motion are deduced. It illustrates the interacting electromagnetic torque and force are opposite to the directions of rotary and axial movements, respectively. For the rotating movement, the interacting torque is related to the axial velocity. Moreover, the axial velocity significantly influences the output torque performances and no-load speed. Similar conclusions can be obtained for axial movement of the helical motion. The 3D finite element method is applied to calculate the exact output performance considering the interacting influence. Furthermore, the prototype machine is manufactured and tested to verify the analytical results.

***Index Terms*— 2-degree-of-freedom motor, Induction motor, Helical motion.**

I. Introduction

Recently, the 2-Degree-of-Freedom (2DoF) direct-drive motor has been considered as an attractive candidate due to the ability of producing rotary, linear or helical motion [1]. In the applications of intelligent machine and mechanical manufacture, it could replace two or more rotary motors and their associated cumbersome mechanisms. And it overcomes the inefficient mechanical driving system for generating complicated motions [2]. Therefore, such 2DoF motor can eliminate the loss of output torque and power during the mechanical transmission process, eventually improve the controllability of the whole driving system. At present, some 2DoF motors have been developed, e.g. induction-type [2-4], permanent-magnet-type [5-7] and reluctance-type [8-10] motors. Due to their integrated structures composed of both rotary and linear motion units, the magnetic interaction between the two units exist. Moreover, extra interaction will be generated between the coexisting rotating and axial movements in helical motion. Then the output performance of the helical motion will be degraded to some extent, which limits the industrial applications of the 2DoF motors. Thus, it is necessary to investigate the motor performance of the helical motion for better design and application.

Presently, some researchers have paid attention to the helical-motion performance and interactions among three motions of 2DoF motors. For the 2-armature 2DoF induction motor, Mandrela revealed the special electromagnetic coupling between the rotary and linear motions using finite element method (FEM) [4]. However, he only investigated the influence of axial motion on rotating motion. For a 2DoF switched reluctance motor, the coupled relationship of the output torque and force was presented from the perspective of decoupled control [8]. Moreover, it was verified that an orthogonal magnetic field in a double stator 2DoF permanent magnet motor led to the connection of rotating and axial movements [7], but the effects of the interaction between the two motions were not considered.

Thus, in this paper, a 2DoF split-stator induction motor (2DoFSSIM) [3] which features compact and simple structure, high environmental adaptability, and high reliability is investigated aiming to study the helical motion performance. The 2DoFSSIM is composed of two arc-shape stators, and a common ferromagnetic mover, which can realize rotary, linear or helical motion, (Fig. 1). The rotary-motion arc-shape stator (RMS) and the mover constitute the rotary motion unit, and the linear-motion arc-shape stator (LMS) as well as the mover form the linear motion unit. The RMS is laminated by silicon laminations slotted in axial direction and the LMS is laminated in circumferential direction. The mover is a solid steel cylinder coated with a layer of cooper. The main structural parameters are listed in Table I.

In this paper, the interacting resistant and output torque and force equations of helical motion of the 2DoFSSIM are explored based on analytical method and 3D FEM. The influences of rotary and linear motion units on each other are considered. The experimental tests are furtherly conducted to verify the existence of such influences.

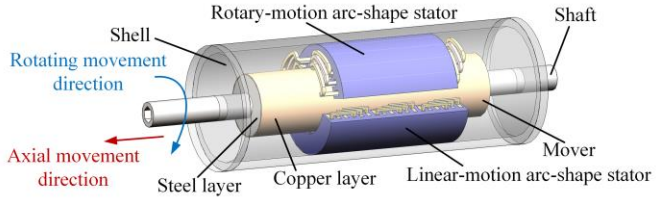

Fig. 1. Topology of the 2DoFSSIM

TABLE I
Main Structural Parameters of the 2DoFSSIM

Items	Rotary Motion Unit	Linear Motion Unit
Slot number N_s/ Pole pair N_r	12/2	
Stator inner diameter D_{si} (mm)	98	
Stator outer diameter D_{so} (mm)	155	
Air-gap thickness g (mm)	2.5	
Rotor outer diameter D_{ro} (mm)	96	
Copper layer length h_{Cu} (mm)	1	
Stator axial length l_a (mm)	135	156
Frequency f (Hz)	50	
Synchronous speed	750r/min	3.92m/s

II. Interacting Force in Helical Motion

The analysis of helical motion characteristics is developed in rectangular coordinate system as shown in Fig. 2. The following assumptions have been made: 1). The end effect is ignored. 2). The curvature of the mover is ignored. 3). Stator windings are replaced by the infinite thin current sheets. 4). Only fundamental components are considered.

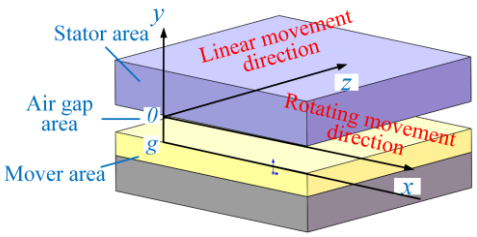

Fig. 2. Expanded view of motions of the 2DoFSSIM.

When the mover generates rotating movement, the speed $\vec{V}$ only has the circumferential component V_x (Peripheral speed), meanwhile, the armature reaction flux B_x, and the induced voltage E_x are produced. Similarly, when the mover produces linear motion, only the axial components V_z, B_z and E_z exist. For helical motion, the speed $\vec{V}$ is composed of V_x and V_z, and additional B_y and E_y are produced, i.e. $\vec{B}=B_x\vec{i}+B_y\vec{j}+B_z\vec{k}$ and $\vec{E}=E_x\vec{i}+E_y\vec{j}+E_z\vec{k}$.

The electromagnetic force density can be calculated as:

$$\vec{F}=\vec{J}\times\vec{B} \tag{1}$$

where, $\vec{J}$ is the current density, $\vec{J}=\sigma(\vec{E}+\vec{V}\times\vec{B})$ and σ is the conductivity. Thus, $\vec{F}$ can be deduced as:

$$\begin{aligned}\vec{F}&=\sigma(\vec{E}+\vec{V}\times\vec{B})\times\vec{B}=\sigma(-\frac{\partial\vec{A}}{\partial t}\times\vec{B}+\vec{V}\times\vec{B}\times\vec{B})\\&=\sigma(\begin{vmatrix}\vec{i}&\vec{j}&\vec{k}\\B_x&B_y&B_z\\\frac{\partial A_x}{\partial t}&\frac{\partial A_y}{\partial t}&\frac{\partial A_z}{\partial t}\end{vmatrix}+\begin{vmatrix}\vec{i}&\vec{j}&\vec{k}\\-V_zB_y&-V_xB_z+V_zB_x&V_xB_y\\B_x&B_y&B_z\end{vmatrix})\\&=\sigma(-V_xB_z^2+V_zB_xB_z-V_xB_y^2+B_y\frac{\partial A_z}{\partial t}-B_z\frac{\partial A_y}{\partial t})\vec{i}\\&+\sigma(B_z\frac{\partial A_x}{\partial t}-B_x\frac{\partial A_z}{\partial t}+V_xB_xB_y+V_zB_yB_z)\vec{j}\\&+\sigma(-V_zB_y^2+V_xB_xB_z-V_zB_x^2+B_x\frac{\partial A_y}{\partial t}-B_y\frac{\partial A_x}{\partial t})\vec{k}\end{aligned} \tag{2}$$

where $\vec{A}$ is the magnetic vector potential, $\vec{A}=A_x\vec{i}+A_y\vec{j}+A_z\vec{k}$. For the 1DoF rotary motion, $V_z=B_z=A_x=A_y=0$, thus the electromagnetic torque is

$$\vec{F_x}=\sigma(-V_xB_y^2+B_y\frac{\partial A_z}{\partial t})\vec{i}+\sigma(-B_x\frac{\partial A_z}{\partial t}+V_xB_xB_y)\vec{j} \tag{3}$$

For the 1DoF linear motion, $V_x=B_x=A_z=A_y=0$, thus the electromagnetic force is

$$\vec{F_z}=\sigma(B_z\frac{\partial A_x}{\partial t}+V_zB_yB_z)\vec{j}+\sigma(-V_zB_y^2-B_y\frac{\partial A_x}{\partial t})\vec{k} \tag{4}$$

Hence, the interacting electromagnetic force in helical motion can be expressed as:

$$\begin{aligned}\Delta\vec{F}&=\vec{F}-\vec{F_x}-\vec{F_z}\\&=\sigma(-V_xB_z^2+V_zB_xB_z-B_z\frac{\partial A_y}{\partial t})\vec{i}\\&+\sigma(V_xB_xB_z-V_zB_x^2+B_x\frac{\partial A_y}{\partial t})\vec{k}\end{aligned} \tag{5}$$

The influences of electromagnetic performance by the interacting electromagnetic force $\Delta\vec{F}$ are investigated from two perspectives, namely rotating and axial movements, which will produce interacting resistant force or torque on each other.

A. *Perspective of the rotating movement*

From the perspective of the rotating movement under helical motion condition, it is assumed that the stator current only follows the direction of z axis and an additional axial movement is presented on the rotating movement of the mover.

Hence, the vector magnetic potential $\vec{A}_r$ in the mover keeps the motion along z axis direction, namely $\partial\vec{A_r}/\partial z=0$ (the subscript r represents that the parameters are derived from the perspective of the rotating movement of the helical motion). The current densities J_r can be expressed by $J_r=J_{mr}\exp[j(\omega_r t-\beta_r x)]$ and the rotating air-gap flux density B_{yr} is represented as $B_{yr}=B_{mr}\exp[j(\omega_r t-\beta_r x)]$. J_{mr} and B_{mr} are the amplitudes, ω_r is the angular speed, $\beta_r=\pi/\tau_r$, τ_r is the pole distance of the rotary motion unit. According to Maxwell's equations as well as the definition of vector magnetic potential $\vec{A}$ ($\vec{B}=\nabla\times\vec{A}$, $\nabla\bullet\vec{A}=0$), (6) and (7) are derived:

$$\nabla^2\vec{A}=\mu\sigma(\frac{\partial\vec{A}}{\partial t}-\vec{V}\times(\nabla\times\vec{A})) \tag{6}$$

$$\begin{cases}\nabla^2A_{xr}=\mu\sigma\left[\frac{\partial A_{xr}}{\partial t}-V_z\frac{\partial A_{zr}}{\partial x}\right]\\\nabla^2A_{yr}=\mu\sigma\left[\frac{\partial A_{yr}}{\partial t}-V_z\frac{\partial A_{zr}}{\partial y}+V_x(\frac{\partial A_{yr}}{\partial x}-\frac{\partial A_{xr}}{\partial y})\right]\\\nabla^2A_{zr}=\mu\sigma\left[\frac{\partial A_{zr}}{\partial t}+V_x\frac{\partial A_{zr}}{\partial x}\right]\end{cases} \tag{7}$$

Combing the boundary conditions (8), the $\vec{A}_r$ in the mover can be obtained as (9), where the subscripts 1 and 2 represent the areas of air gap and mover (Fig. 2).

$$\begin{cases}H_{1xr}=-J_r\\A_{1xr}=A_{1yr}=0\end{cases},\ y=0$$

$$\begin{cases}B_{1yr}=B_{2yr}\\H_{1xr}=H_{2xr}\end{cases},\ y=g \tag{8}$$

$$A_{2xr}=A_{2yr}=A_{2zr}=0,\ y\to\infty$$

$$\begin{cases}A_{2xr}=-\frac{V_zB_{mr}}{V_xj\beta_r\gamma_r}e^{-\alpha_{zr}(y-g)}e^{j(\omega_rt-\beta_rx)}\\A_{2yr}=j\frac{\beta_r}{\alpha_{zr}}\frac{V_zB_{mr}}{V_xj\beta_r\gamma_r}e^{-\alpha_{zr}(y-g)}e^{j(\omega_rt-\beta_rx)}\\A_{2zr}=\frac{B_{mr}}{j\beta_r\gamma_r}e^{-\alpha_{zr}(y-g)}e^{j(\omega_rt-\beta_rx)}\end{cases} \tag{9}$$

where, $\gamma_r=\mathrm{ch}(\beta_rg)+\alpha_{zr}\mu\,\mathrm{sh}(\beta_rg)/(\beta_r\mu)$, $\alpha^2{}_{zr}=\beta^2{}_r+js_r\omega_r\mu\sigma$, g is the thickness of the air gap, s_r is the slip of rotary motion, μ and σ represent the permeability and conductivity of the mover. Here,

the attenuation component with attenuation coefficient α_{xr} is ignored to simplify analysis [11]. Then the flux density and current density can be derived. According to (5), the interacting resistant torque produced by the axial movement in the rotating movement can be obtained as

$$\Delta F_{xr} = -j\mu\beta_r \left[s_r V_{1r} \frac{V_z}{V_x} \frac{\sigma B_{mr}}{\alpha_{zr}\beta_r\gamma_r} e^{-\alpha_{zr}(y-g)} \mathrm{e}^{j(\omega_r t-\beta_r x)} \right]^2 \quad (10)$$

where V_{1r} is the synchronous rotating peripheral speed, and the minus sign means that the interacting resistant torque is opposite to the output rotating torque. With the same structural parameters of rotary motion unit and the same rotating speed, the changes of the rotating magnetic field parameters are ignored. Fig. 3 gives the output torque vs. rotating speed curves of the helical motion with different axial velocities derived by 3D FEM. H means both stators are powered, L and R represent axial and rotating movements respectively. The no-load rotating speeds with different axial velocities are derived as shown in Fig. 4. The per unit value of torque is utilized and the based torque is the corresponding locked torque.

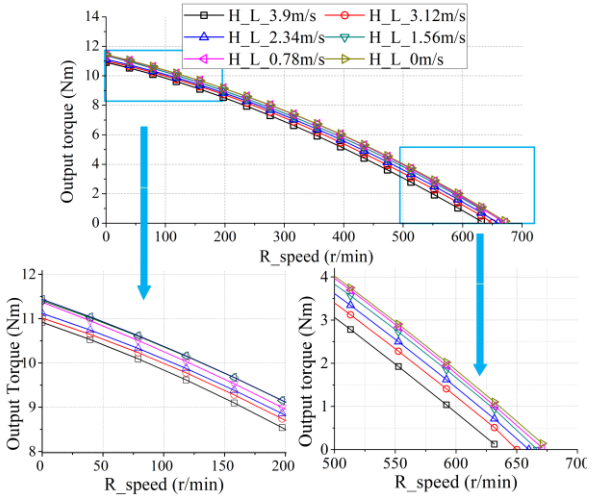

Fig. 3. Torque vs. rotating speed vs. axial velocity of helical motion.

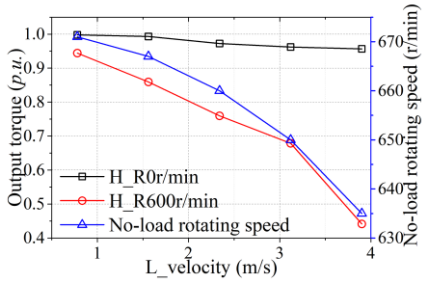

Fig. 4. No-load rotating speed and per-unit value of the output rotating torque vs. axial velocity of helical motion.

Therefore, some rotating characteristics of the helical motion can be predicted according to (10), which are then verified by the results of 3D FEM:

1). The interacting resistant torque ΔF_{xr} increases with the increase of the axial velocity V_z, and the corresponding output rotating torque decreases as shown in Fig. 3.

2). The interacting resistant torque ΔF_{xr} is proportional to V_z^2 at a certain rotating speed, hence the increment of ΔF_{xr} rises with the increase of V_z, e.g. the case of rotating speed 600r/min as shown in Fig. 4.

3). When the rotating movement is locked, i.e. V_x=0, the motor produces 1DoF linear motion, so the equation (10) is not available. Under this situation, ΔF_{xr}=0 and the per unit of locked torque are approximately equal to 1 as shown in Fig. 4. The variations under different axial velocities are tiny. The reason is that the rotating and travelling wave magnetic fields are coupled in the mover.

4). The no-load rotating speed cannot reach the ideal synchronous speed on account of ΔF_{xr} and it decreases with the rise of V_z as shown in Fig. 4.

B. *Perspective of the axial movement*

Similarly, from the perspective of axial movement, the 2DoFSSIM with helical motion can be reckoned that only the stator current in the circumferential direction (equivalent to x axial) exists and the additional rotating movement is presented on the mover. Thus, the vector magnetic potential $\vec{A}_l$ in the mover keeps the same in x axis direction, namely $\partial\vec{A}_l/\partial x = 0$ (the subscript l represents that the parameters are derived from the perspective of the axial movement of the helical motion.). The current densities J_l can be expressed by J_l=J_{ml}exp[$j(\omega_l t$-$\beta_r z)$] and traveling wave air-gap flux density in air-gap B_{yl} is represented as B_{yl}=B_{ml}exp[$j(\omega_l t$-$\beta_l z)$], where, J_{ml} and B_{ml} are the amplitudes, ω_l is the angular speed, β_l =π/τ_l, τ_l is the pole distance of the linear motion unit. Based on the same theory of Part A and replacing the parameters by those derived from the perspective of the axial movement, the the vector magnetic potential can be derived:

$$\begin{cases} A_{2xl} = -\dfrac{V_x B_{ml}}{V_z j\beta_l\gamma_l} e^{-\alpha_{zl}(y-g)} \mathrm{e}^{j(\omega_l t-\beta_l z)} \\ A_{2yl} = j\dfrac{\beta_l}{\alpha_{zl}} \dfrac{V_x B_{ml}}{V_z j\beta_l\gamma_l} e^{-\alpha_{zl}(y-g)} \mathrm{e}^{j(\omega_l t-\beta_l z)} \\ A_{2zl} = \dfrac{B_{ml}}{j\beta_l\gamma_l} e^{-\alpha_{zl}(y-g)} \mathrm{e}^{j(\omega_l t-\beta_l z)} \end{cases} \quad (11)$$

where, γ_l=ch($\beta_l g$)+$\alpha_{zl}\mu$sh($\beta_l g$)/($\beta_l\mu$), α^2_{zl}=β^2_l+$js_l\omega_l\mu\sigma$, and s_l is the slip of axial motion. According to (5), the interacting resistant torque produced by the rotating movement in the linear motion can be obtained as

$$\Delta F_{xl} = -j\mu\beta_l \left[s_l V_{1l} \frac{V_x}{V_z} \frac{\sigma B_{ml}}{\alpha_{zl}\beta_l\gamma_l} e^{-\alpha_{zl}(y-g)} \mathrm{e}^{j(\omega_l t-\beta_l z)} \right]^2 \quad (12)$$

where V_{1l} is the synchronous axial velocity and the direction of the interacting resistant force is opposite to that of the output axial force. In a same way with that of the rotating movement, the similar trends of interacting resistant force, no-load axial velocity and output axial force with rotating speed can be predicted.

The force vs. axial velocity curves of the helical motion and no-load axial velocities with different rotating speeds derived by 3D FEM are shown in Figs. 5 and 6, where the per-unit values of the forces are also utilized to analyze the force performance influenced by the ΔF_{xl}. It can be found that the output force decreases with the increase of the rotating speed

of the helical motion, and the decrement of the output force also keep increasing. In addition, the locked forces at different rotating speeds are approximately identical, and the no-load axial velocity decreases as the rotating speed rises, which is less than the ideal synchronous velocity of 3.92m/s due to the existence of ΔF_{xl}.

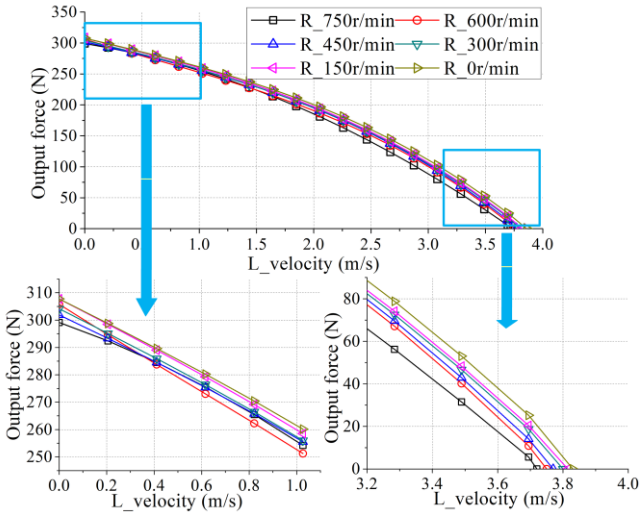

Fig. 5. Force vs. axial velocity vs. rotating speed of the helical motion.

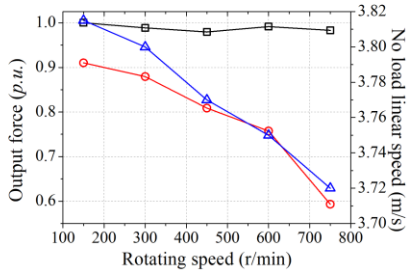

Fig. 6. No-load axial velocity and per-unit value of the output axial force vs. rotating speed of helical motion.

III. Experimental Verification

The prototype testing platform system was built (shown in Fig. 7) and experimental tests were carried out.

Fig. 7. Prototype of the 2DoFSSIM.

Firstly, the RMS is powered with 133V-30Hz AC source, while the LMS is not powered, and there is no additional load on the mover. Then at $t=t_0$, the LMS was supplied with voltage source (90V-20Hz) to investigate the influences of rotating movement by the axial movement as shown in Fig. 8. It can be found that the experimental results agree well with the 3D FEM results. For the rotary motion without axial movement, the rotating speed was derived as 381.72r/min, which is less than the ideal value (450r/min). Since the mechanical friction exists, the actual load acting on the mover is higher than 0. Then for the rotary motion with axial movement after t_0, the rotating speed of the helical motion reduced to 323.78r/min, which is 15.18% smaller than the value without axial movement. Therefore, the performance of the helical motion is deteriorated compared with the corresponding 1DoF rotary motion, which validates the results of theoretical analysis.

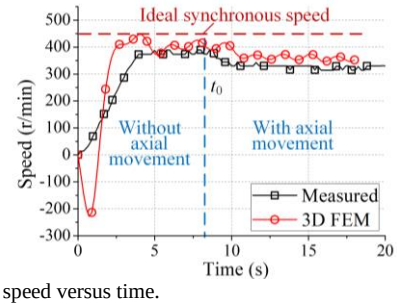

Fig. 8. Rotating speed versus time.

IV. Conclusion

In this paper, the torque and thrust predictions for the helical motion of the 2DOFSSIM are presented based on theoretical analysis. The interacting resistant force in the helical motion is investigated. It shows that a resistant rotating torque caused by the axial movement degrades the output torque of the rotating movement and resistant effect grows as the axial velocity increases. The no-load speed also decreases due to such resistant torque. Similarly, the same phenomenon exists for the axial movement, which is caused by the rotating movement. The 3D FEM results and experimental tests verify the correctness of analytical results.

References

[1] L. Szabó, "On the use of rotary-linear generators in floating hybrid wind and wave energy conversion systems," in *IEEE Int. Conf. AQTR*, Romania, pp. 1-6, 2018.

[2] M. Rabiee and J. J. Cathey, "Verification of a field-theory analysis applied to a helical motion induction-motor," *IEEE Trans. Magn.*, vol. 24, no. 4, pp. 2125-2132, Jul 1988.

[3] J. Si, H. Feng, L. Ai, Y. Hu, and W. Cao, "Design and analysis of a 2-DOF split-stator induction motor," *IEEE Trans. on Energy Convers.*, vol. 30, no. 3, pp. 1200-1208, 2015.

[4] E. Amiri, M. Jagiela, O. Dobzhanski, and E. Mendrela, "Modeling dynamic end effects in rotary armature of rotary-linear induction motor," *in IEEE Int. Conf. IEMDC*, USA, pp.12-15, 2013.

[5] P. Jin, H. Lin, S. Fang, and S. L. Ho, "Decoupling control of linear and rotary permanent magnet actuator using two-directional d-q transformation," *IEEE Trans. Magn.*, vol. 48, no. 10, pp. 2585-2591, Oct 2012.

[6] S. Fang, K. Guo, H. Lin, D. Wang, and H. Yang, "Electromagnetic analysis of a HTS linear-rotary permanent magnet actuator," *IEEE Trans. Appl. Supercon.*, vol. 26, no. 7, pp. 1-5, Oct 2016.

[7] L. Xu, M. Lin, X. Fu, X. Zhu, C. Zhang, and W. Wu, "Orthogonal magnetic field analysis of a double stator linear-rotary permanent magnet motor with orthogonally arrayed permanent magnets," *IEEE Trans. Magn.*, vol. 53, no.11, pp.2501104, 2017.

[8] J. F. Pan, Y. Zou, and N. C. Cheung, "Performance analysis and decoupling control of an integrated rotary-linear machine with coupled magnetic paths," *IEEE Trans. Magn.*, vol. 50, no. 2, pp. 761-764, 2014.

[9] Y. Sato, K. Murakami, and Y. Tsuboi, "Sensorless torque and thrust estimation of a rotational/linear two degrees-of-freedom switched reluctance motor," *IEEE Trans. Magn.*, vol. 52, no. 7, pp. 1-4, 2016.

[10] S. Li, K. W. E. Cheng, J. Zhu, and Y. Zou, "Design and application of a decoupled rotary-linear switched reluctance motor for concentrated photovoltaic power generation," *IET Electric Power Appl.*, vol. 12, no. 7, pp. 908-915, 2018.

[11] S. Yamamura, "Theory of linear induction motors," *New York, Halsted Press, 1979. 246 p.*, 1979.